ACS APPLIED MATERIALS & INTERFACES

Research Article

www.acsami.org

A Green Approach for Preparing Doped TiO_2 Single Crystals

Lu-Lu Long, Ai-Yong Zhang,* Jun Yang, Xing Zhang, and Han-Qing Yu*

CAS Key Laboratory of Urban Pollutant Conversion, Department of Chemistry, University of Science & Technology of China, Hefei, 230026, China

Supporting Information

ABSTRACT: Doped TiO_2 with metal, nonmetal, and rare earth elements has shown a great potential in energy and environmental applications, but it is difficult to dope well-defined TiO_2 single crystals (SCs) with {001} exposed facet due to their high crystallinity. In this work, we developed a green and general approach to prepare the {001}-exposed TiO_2 SCs doped with various elements, on the basis of recycling the wasted ethylene glycol electrolyte from the anodic oxidation for TiO_2 nanotube preparation. All six representative elements (i.e., metal, nonmetal, and rare earth types) could be successfully doped into the TiO_2 SCs without breaking their single-crystalline structure and exposed high-energy facet. The electronic properties of the doped TiO_2 SCs were significantly improved. All the doped TiO_2 SCs exhibited a superior photoactivity under visible-light irradiation for degrading rhodamine B, a typical organic pollutant. The prepared doped TiO_2 SCs have a promising potential in environmental and energy applications.

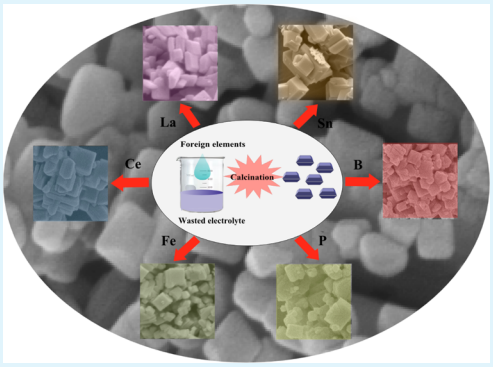

KEYWORDS: *doping, {001}-exposed facet, single crystal, photocatalytic activity, titanium dioxide (TiO_2)*

INTRODUCTION

Due to the intrinsic crystal structure and semiconducting properties, pure TiO_2 possesses a large band gap, low electric conductivity, poor photochemical and electrochemical properties, and slow charge mobility (electronic structure/electronic properties). These drawbacks have largely limited its efficient and cost-effective applications in photocatalysis, water splitting, dye-sensitized solar cells, lithium-ion batteries, and so on.[1] On the other hand, owing to the typical electronic configuration of Ti^{4+}, it is possible to tailor the band gap, electric conductivity, and optoelectronic properties of TiO_2 by preferential doping with *s*, *p*, *d*, or *f* block elements in the lattice structure. Thus, many recent works have been conducted to solve the aforementioned intrinsic problems by changing the electronic structure of the TiO_2 via impurity doping from crystal engineering, and various doping methods are able to accommodate the dopants in different positions within structure. The doped TiO_2 catalysts usually show superior performance in energy and environmental applications because of their significantly improved crystal structures and physicochemical properties.[2] For example, nitrogen atoms are substituted for the lattice oxygen sites, narrowing the band gap by mixing the N 2p and O 2p states and resulting in an enhanced photoactivity in the visible region.[3]

TiO_2 can be doped mainly by three types of foreign atoms: nonmetals (S, C, Br, B, etc.),[3−7] transition metals (W, Co, V, Sn, etc.),[8−12] and rare earth metals (Sm^{3+}, Ce^{3+}, Er^{3+}, La^{3+}, Nd^{3+}, etc.),[13−17] and different elements endow TiO_2 with diverse properties. These doped foreign atoms might bring about four significant effects: (1) narrow the large band gap to extend responsive spectra into the visible light range, and obtain satisfactory photocatalytic activity under visible light irradiation (e.g., doping of N, S, I and B);[18] (2) enhance electric conductivity and charge mobility to decrease the invalid recombination in bulk and on TiO_2 surface, improve the separation and transfer of the active photocarriers, and prolong their effective lifetime (e.g., doping of Zn, Fe, and Y);[19−21] (3) change the conduction band position of the TiO_2 negatively and positively, and influence the charge transport properties (e.g., doping of Zr^{4+}, Nb^{5+}, and W^{6+}); and (4) increase the overall photochemical and electrochemical activities and application performance because of the enhanced electron transport and lower exciton recombination rate.[22,23] Therefore, foreign doping has become one of the most important strategies to improve the overall performance and extend the application fields of TiO_2.

It has been well documented that TiO_2 surface and catalytic properties are also closely associated with its crystal structures and exposed facets.[24] The anatase TiO_2 single crystals (SCs) exposed by high-energy {001} facet have attracted increasing interests because of their high performance, low cost, and nontoxicity.[25] The thermodynamically unstable {001} surface is proven to have a much higher surface energy (0.90 J/cm^2) than the thermodynamically stable {101} surface, which has a lower surface free energy (0.44 J/cm^2).[26] Moreover, the arrangement and category of constituent atoms on high-energy {001} facets govern its unique geometrical and electronic structures, and its surface functional groups considerably affect its stability,

Received: June 11, 2014
Accepted: September 4, 2014
Published: September 4, 2014

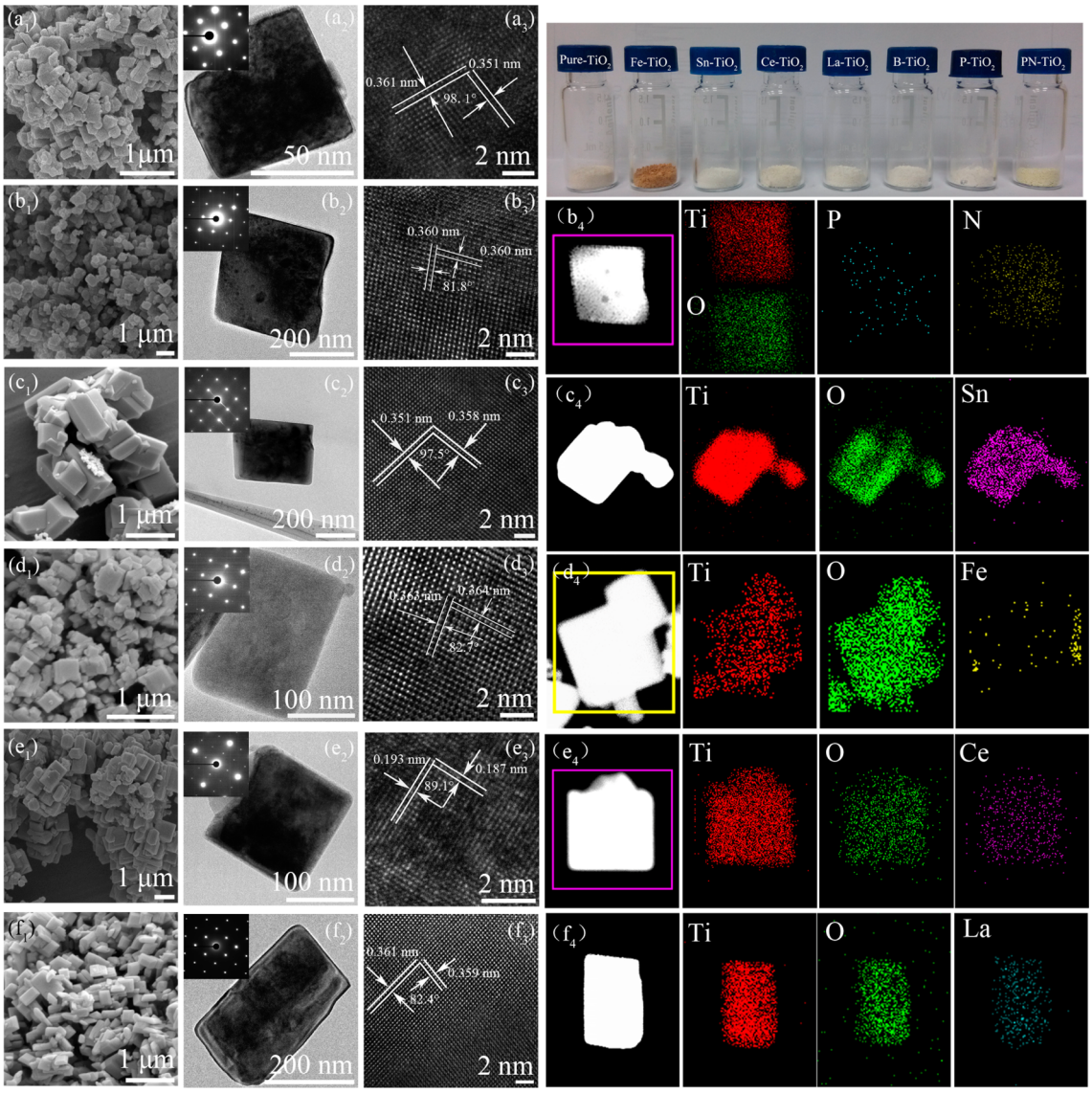

Figure 1. (A, left three columns) SEM and HRTEM images and the corresponding SAED patterns and (B, right four columns) the optical images and elemental mappings (a) of B-TiO_2, (b) P-TiO_2 SCs, (c) Sn-TiO_2, (d) Fe-TiO_2, (e) Ce-TiO_2 and (f) La-TiO_2.

adsorptive property, and catalytic activity.[25] All these features make TiO_2 SCs with {001} facets highly efficient for energy and environmental applications.[25,27]

It is highly desirable to synergistically combine crystal engineering with surface engineering on one single TiO_2 particle to maximize the application potentials. However, it is difficult to incorporate dopants into the well-faceted TiO_2 SCs because of the high crystallinity of the SCs.[28] Moreover, a dose of dopant precursors would inevitably influence the nucleation and growth of TiO_2 crystals.[28−32] In these works, the foreign atoms are doped either from a special precursor, such as TiN, TiC, and $TiOF_2$, or from an additional thermal treatment. Herein, we reported a simple and general approach to prepare the doped TiO_2 single crystal with dominant {001} facets based on the chemical recycling of the wasted and toxic ethylene glycol electrolyte from the widely used anodic oxidation.[33]

In our previous work,[34] both pristine and N-doped TiO_2 SCs have been successfully prepared through recycling such an electrolyte; these crystals exhibited a much higher photocatalytic activity in decomposition of humic acids and bentazone than Degussa P25, one of the best commercial TiO_2 photocatalysts. Apparently, this preparation approach possesses significant economic and environmental benefits, and the doping strategy of TiO_2 SCs is simple and promising. In this study, we further try to expand the use of such a recycling strategy and develop a general approach of prepare the {001}-exposed TiO_2 SCs doped with various metal, nonmetal, and rare earth metal elements. Moreover, a method for codoping different foreign atoms under the appropriate conditions was also established. The photocatalytic capacities of all the doped TiO_2 SCs were examined in terms of degrading rhodamine B (RhB), a widely used azo dye and commonly encountered pollutant, under visible-light irradiation. To our knowledge, this is the first report to develop a general approach to prepare doped and codoped anatase TiO_2 SCs with dominant {001} facets.

EXPERIMENTAL SECTION

Synthesis of the Doped TiO_2 SCs. The synthesis of the doped TiO_2 SCs with exposed {001} facets was performed after simple thermal treatment of the wasted anodic electrolyte, with different

dx.doi.org/10.1021/am503661w | ACS Appl. Mater. Interfaces 2014, 6, 16712−16720

precursors of the target foreign atoms. The wasted anodic electrolyte was yielded as reported previously,[34] and the concentrated sol, which was rich in $[TiF_6]^{2-}$ complex, was used as the precursor solution for TiO_2 preparation. Typically, the anodization process was carried out in a voltage-regulated mode. A homemade two-electrode configuration was adopted, and two Ti foils with the same effective size of 2 × 4 cm were used as anode and cathode, respectively. Initially, two 0.30 mm Ti foils were burnished and immersed in the chemical polishing solution ($HF/HNO_3/H_2O$ = 1:1:2, v/v) to remove the oxide layer and blot, and finally cleaned with soap, acetone, and isopropanol before and after chemical polishing. Later, anodization was conducted in 0.09 M NH_4F solution (prepared using 8 mL of deionized water and 72 mL of ethylene glycol as the mixed solvent) under continuous stirring, with the pretreated two Ti foils as anode and cathode. All electrolytes were prepared from reagent-grade chemicals. The electrochemical treatment was conducted by applying a potential scanning from the open-circuit potential first to 80 V for 2 min, then to 70 V for 2 min, 60 V for 2 min, and 50 V for 2 min; this voltage-regulated process was repeated; and finally, a potential scanning from the open-circuit potential to 40 V was applied for 120 min at ambient temperature (20 ± 3 °C).

To prepare the La-, Ce-, Sn-, Fe-, B-, and P-doped TiO_2 crystals, we added 0.05 mL of lanthanum nitrate solution (0.1 M), 0.05 mL of cerous nitrate solution (0.1 M), 5 mL of stannous chloride solution (0.1 M), 0.5 mL of ferric nitrate solution (1 M), 2 mL of boracic acid solution (1 M), and 0.5 mL of phosphoric acid solution (1 M) individually into this anodic electrolyte, followed by sonication for 15 min. Finally, the homogeneously mixed sol solution was transferred to a combustion boat and annealed in air at 500 or 600 °C for 3 h to yield the final doped products. In a typical procedure, 10 mL of concentrated wasted anodic electrolyte (sol) with a solid concentration of ca. 48 g L^{-1} after ultrasonic treatment was calcinated at 500 or 600 °C for 3 h with a ramping rate of 3 °C/min, and approximately 0.25 g of colored or white powders could be obtained after being cooled to room temperature.

Characterization. The morphology and structure of the TiO_2 crystals were characterized by field-emission scanning electron microscope (FE-SEM; SIRION200, FEI Co., The Netherlands), high-resolution transmission electron microscope and selected-area electron diffraction (HRTEM/SAED; JEM-2100, JEOL Co., Japan) and scanning transmission electron microscope (STEM; JEM-ARM200F, JEOL Co., Japan). The surface area was measured by using the Brunauer–Emmett–Teller method with a Builder 4200 instrument (Tristar II 3020M, Micromeritics Co.) at liquid nitrogen temperature. X-ray diffraction (XRD; X'Pert, PANalytical BV, The Netherlands) was used to analyze the crystal structure. The diffuse reflectance spectra (DRS) were measured using a UV–vis spectrophotometer (UV 2550, Shimadzu Co., Japan). The chemical compositions were characterized by energy dispersive X-ray analyzer (EDX; GENESIS, EDAX Co.) fitted to the SEM chamber and X-ray photoelectron spectroscopy (XPS; PHI 5600, PerkinElmer Inc.), respectively.

All electrochemical measurements were carried out in a homemade three-electrode system with pure and modified TiO_2 SCs deposited on glassy carbon electrode as the working electrode, Pt wire as the counter electrode, and Ag/AgCl as the reference electrode. Electrochemical impedance spectroscopy (EIS) was conducted by applying an AC voltage amplitude of 5 mV within the frequency range of 10^5 to 10^{-2} Hz in 10 g/L NaCl aqueous solution under the open-circle potential (OCP); Mott–Schottky plots were obtained in 0.1 M Na_2SO_4 aqueous solution by impedance measurement at the fixed frequency of 1000 Hz between the applied voltage range of −0.50 to 1.0 V; oxygen evolution reaction was carried out in 0.1 M KOH aqueous solution at a scan rate of 50 mV s^{-1}.

Photocatalytic Tests. The photocatalytic properties of the TiO_2 crystals were evaluated in a homemade photoreactor by short-circuit photocurrent from a conventional three-electrode system and the decolorization of RhB in aqueous solution under visible light irradiation (λ > 420 nm). An aqueous solution containing 20 mL of 5 mg L^{-1} dye and 20 mg of TiO_2 was magnetically stirred in the dark for 20 min and then exposed to a 500 W xenon lamp (PLS-SXE500, Beijing Trusttech Co., China) equipped with a 420 nm cutoff filter. After irradiation for a designated time, aliquots were taken from the irradiated reaction container and subjected to centrifugation to separate TiO_2 particles. RhB concentration was monitored by the absorbance value at the maximum peak (554 nm) by using a UV–visible spectrophotometer (UV-2450, Shimadzu Co., Japan).

RESULTS AND DISCUSSION

Morphology and Structure of the Doped TiO_2 SCs. Figure 1A shows the typical SEM images of {001}-exposed TiO_2 SCs doped by La, Ce, Sn, Fe, B, and N prepared at 600 °C. All the doped crystals exhibited a well-defined truncated octahedral bipyramid with eight {101} facets and two {001} facets. Compared to the pristine TiO_2 crystals, the foreign doping significantly changed their morphologies. The average sizes of the pristine and the modified TiO_2 crystals doped by La, Ce, Sn, Fe, and B remained at 200–300 nm, but sizes decreased to 50–100 nm when doped by P, which might be attributed to the fact that P atom dopants drastically influenced crystalline growth.[35] In comparison with morphology, their structural characteristics were not changed by the foreign doping, and all six doped samples exhibited an intrinsic single-crystalline structure as determined from the corresponding SAED patterns, matching the pristine one well (Figure 1A).

The HRTEM results further reveal good crystalline and clear lattice fringes of these doped crystals (Figure 1A). The continuous lattice fringes with an interplanar lattice spacing of 0.36 nm and an angle of nearly 90° fit well with the (101) atomic planes of the anatase TiO_2 SCs. It should be mentioned that the lattice spacing of all these doped crystals intrinsically consisted with the pristine analogue without any foreign doping. This might be mainly because of both the very small doping level (~1%) as determined from the XPS results and their highly dispersed behaviors evidenced by the STEM imaging (Table S1, Supporting Information). The STEM elemental mapping was performed to further explore the geometric distribution of these foreign atoms in the doped TiO_2 SCs, and the corresponding elemental maps exhibited their highly uniform distribution over the entire volume of the sphere (Figure 1B). Moreover, the synergistic codoping could also be obtained using this approach under appropriate conditions (Figure 1B).

The XRD analysis was used to examine the crystal structure of both the pristine and the doped samples. The measured diffraction peaks of all samples matched well those of intrinsic anatase TiO_2 (JCPDS No.21-1272), and no residual phase could be detected (Figure 2, top). For example, the two broad peaks at 25.4° and 48.1° could be attributed to the {101} and {200} plane, respectively. Moreover, the difference in the peak intensities at 25.32° {101} and 37.93° {004} for both the pristine and doped TiO_2 samples could be mainly related to the preferential crystallographic orientation of the crystal facets exposed. These results illustrate that the impurity doping did not alter the TiO_2 crystalline type. The XRD patterns confirm that almost no peak shift occurred because of their low doping level and high dispersion. It is difficult for La^{3+} to enter into the TiO_2 lattice structure because of the larger size of La^{3+} (0.115 nm) than that of Ti^{4+} (0.068 nm). Thus, the formation of structural defect was less, the lattice parameters of doped TiO_2 SCs would not change, and almost no distortion took place, ascribed to the mismatch of the two ionic radii. However, it should also be noted that the low sensitivity of the XRD might

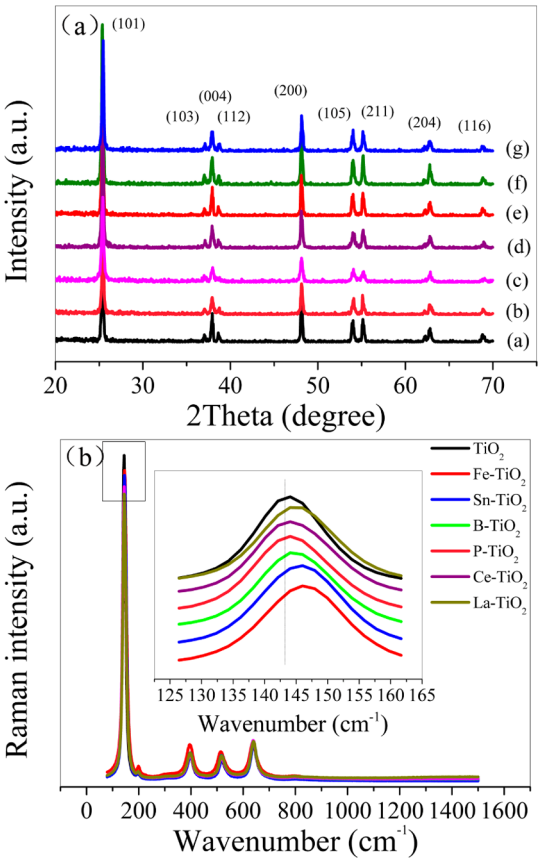

Figure 2. (Top, a) XRD and (bottom, b) Raman spectra of the pure and doped TiO_2 SCs: (a) TiO_2, (b) La-TiO_2, (c) Ce-TiO_2, (d) Fe-TiO_2, (e) Sn-TiO_2, (f) B-TiO_2 and (g) P-TiO_2.

prevent observing the separate impurity phase in the doped TiO_2 SCs because of the added low concentrations of the precursor. For example, the Ce^{4+}/Ce^{3+} with a large ion size was proven to mainly rest on the surface or grain boundaries of the particles.

The Raman spectra indicate that all the samples calcined at 450 °C were present in pure anatase phase corresponding to the characteristic peaks around 144 cm^{-1} (B_{1g}), 394 cm^{-1} (B_{1g}), 514 cm^{-1} (E_g), and 638 cm^{-1} (E_g), except for the expressed 147 cm^{-1} (E_g) (Figure 2, bottom). No effect of impurity doping was observed on the position of peaks in Raman spectra, and the intrinsic anatase structure was integrally retained after doping with different dopants. Moreover, the variation of the foreign atoms resulted in a slight red shift of the principal peaks, which could be attributed to the enhanced crystallization degree of anatase and more surface oxygen vacancies and/or crystal defects due to the difference in chemical state and ionic radii between the Ti host and the doping guest. These effects could reduce the recombination between photoelectrons and holes, as both oxygen vacancies and crystal defects could capture photoelectrons, leading to a higher quantum efficiency.[36] Similarly, the presence of La_2O_3 and Ce_2O_3 could also trap photoelectrons and thus reduce their recombination with holes, which could be attributed to the distortion of anatase crystalline lattice from the interstitial doping. This resulted in an enhanced photoactivity.

XPS analysis was performed to examine the chemical nature and atomic concentration of foreign dopants in TiO_2 SCs (Figure 3). There was no obvious chemical shift of electron binding energies for Ti 2p and O 1s peaks of the all-doped crystals. However, the target foreign atoms all exhibited their corresponding chemical states. Moreover, if the electronegativity and ionic radius of the doping ions matched those of the lattice ions in the oxide, the lattice ions could be substituted by the doping ions in the sample preparation process. For nomental B doping, the peak at around 191.9 eV could be ascribed to Ti−O−B bond, much lower than that in either the pure B_2O_3 (193.9 eV) or the H_3BO_3 (193.5 eV), suggesting the successful doping into the interstitial TiO_2 structure, rather than in a separate phase (Figure 3a). In addition, the no shift of the Ti might be ascribed to its relatively greater atomic weight.[37]

For the doping of nonmetal P, the P 2p3/2 binding energy at around 133.3 eV suggests that the P was in a P^{5+} oxidation state, probably in the form of Ti−O−P, as identified by the FT-IR result (Figure S1, Supporting Information). This indicates that P was likely to be incorporated as a cation and replace Ti ion in the P-doped TiO_2 crystals (Figure 3b). For the modified titania, doping with nonmetal cationic species (i.e., S^{6+}, I^{5+} and P^{5+}) has attracted considerable interest recently.[4,18,30,31,35,38] The band gap narrowing in this type of impurity-doped TiO_2 should be similar to the situation of conventional transition-metal ion doping.[38] The presence of P increased the crystallization temperature of TiO_2 and suppressed the phase transformation from anatase to rutile and the growth of TiO_2 crystallites, leading to a higher surface area of the P-doped TiO_2, and consequently granted them a higher content of surface hydroxyl groups.

For metal Sn doping, the doublet peaks at 486.6 and 494.9 eV in the Sn 3d spectra could be ascribed to the Sn 3d5/2 and Sn 3d3/2 of the substitutional Sn^{4+} dopants in the lattice, confirming the formation of a Sn−O−Ti linkage in the Sn-doped TiO_2 crystals (Figure 3c).[12,39] Because the ionic radius of Sn^{4+} (0.69 Å) is slightly larger than that of lattice Ti^{4+} (0.53 Å), the lattice parameters, cell volume, and *d* values of TiO_2 increased after doping, while the decreased crystal size of the doped TiO_2 should be attributed to the suppressed growth of crystal grains because of the dissimilar boundaries.[39] On the other hand, because of their similar sizes, the substitution of Ti^{4+} in the lattice by Fe^{3+} was favored. The Fe 2p from the doped TiO_2 SCs exhibited the binding energies at 710.5 and 723.7 eV, which were ascribed to the Fe 2p3/2 and Fe 2p1/2 of the standard Fe_2O_3 (Figure 3d). A small lattice expansion occurred due to the elongation of the *c* parameter of tetragonal cell, resulting from the compensating effects between iron substitution of titanium and oxygen vacancy formation to maintain charge neutrality.[40]

For the doping of rare earth metal La, only La_2O_3 adsorbed on TiO_2 was detected. The binding energies at 836.3 and 853.6 eV in the La-doped TiO_2 sample could be attributed to the La 3d5/2 and La 3d3/2 in the form of La_2O_3,[41] and no significant influence of the presence of La_2O_3 on the Ti_{2P} level was observed, implying that no Ti−La bonding was formed (Figure 3e). In addition, the La_2O_3−TiO_2 exhibited three peaks around 529.0, 531.0, and 532.4 eV in the O 1s spectrum, corresponding to the Ti−O, surface H−O, and La−O bonds, respectively.[41] The XPS results further indicate that the La_2O_3 was present in a separate phase adsorbed by TiO_2, rather than being incorporated into TiO_2 lattice via Ti−O−La linkage. Furthermore, the La-modified TiO_2 exhibited a significant improvement in both the photocatalytic activity and thermal stability.

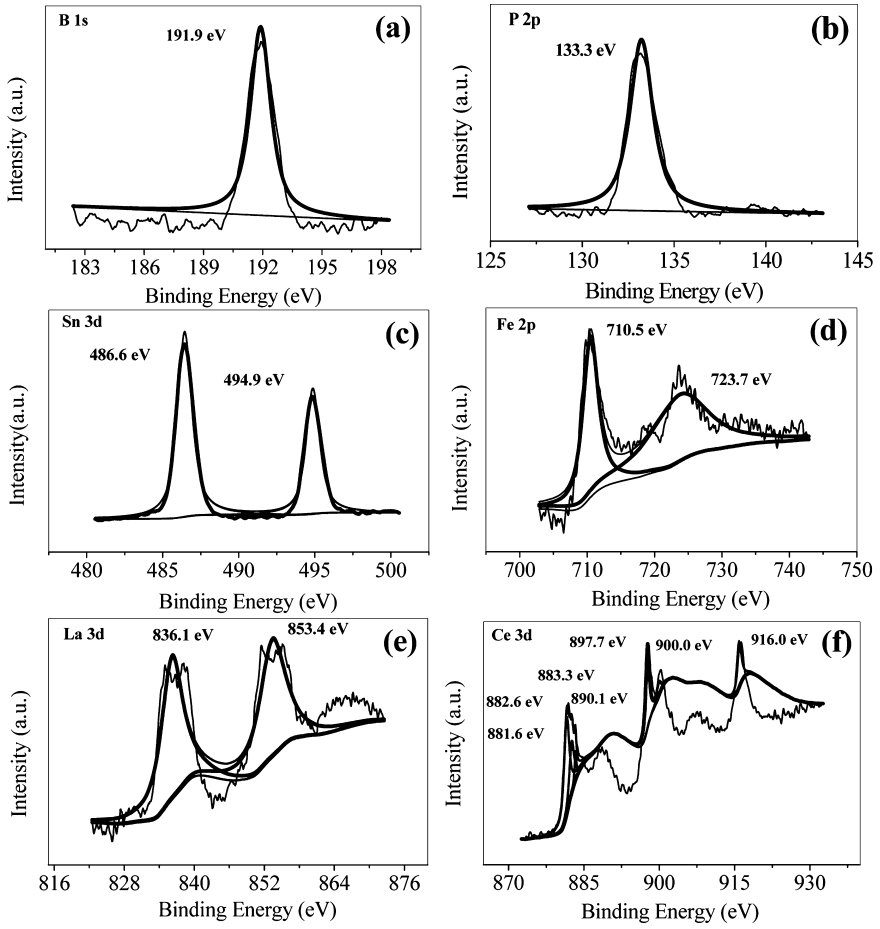

Figure 3. XPS spectra of the doped TiO_2 SCs prepared at 600 °C: (a) B-TiO_2, (b) P-TiO_2, (c) Sn-TiO_2, (d) Fe-TiO_2, (e) La-TiO_2, and (f) Ce-TiO_2.

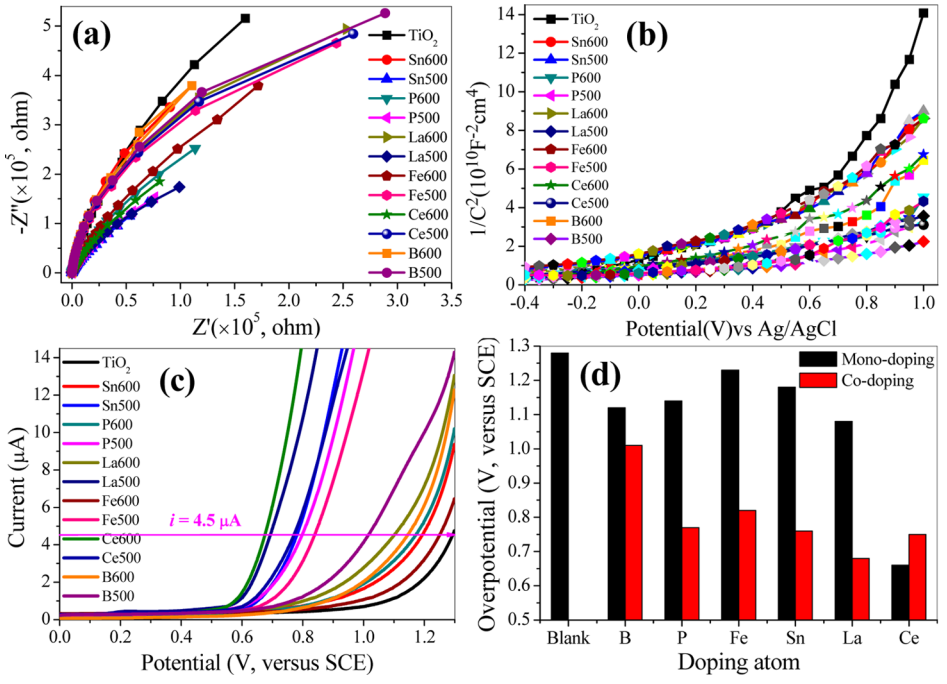

Figure 4. (a) EIS spectra, (b) Mott–Schottky spectra, (c) OER, and (d) the corresponding overpotentials at the selected 0.45 μA.

In the case of doping of rare earth metal Ce, the binding energies at 882.6, 890.1, and 897.7 eV were attributed to the primary photoemission of Ce 3d from the Ce-doped TiO_2; the peak at 881.6 eV was ascribed to a mixture of $(5d\ 6s)^0 4f^2 O\ 2p^4$ configuration in Ce_2O_3; the peak at 900.0 eV showed the partial oxidation of Ce^{3+}; and the diffraction peaks for Ce_2O_3 were not

dx.doi.org/10.1021/am503661w | ACS Appl. Mater. Interfaces 2014, 6, 16712−16720

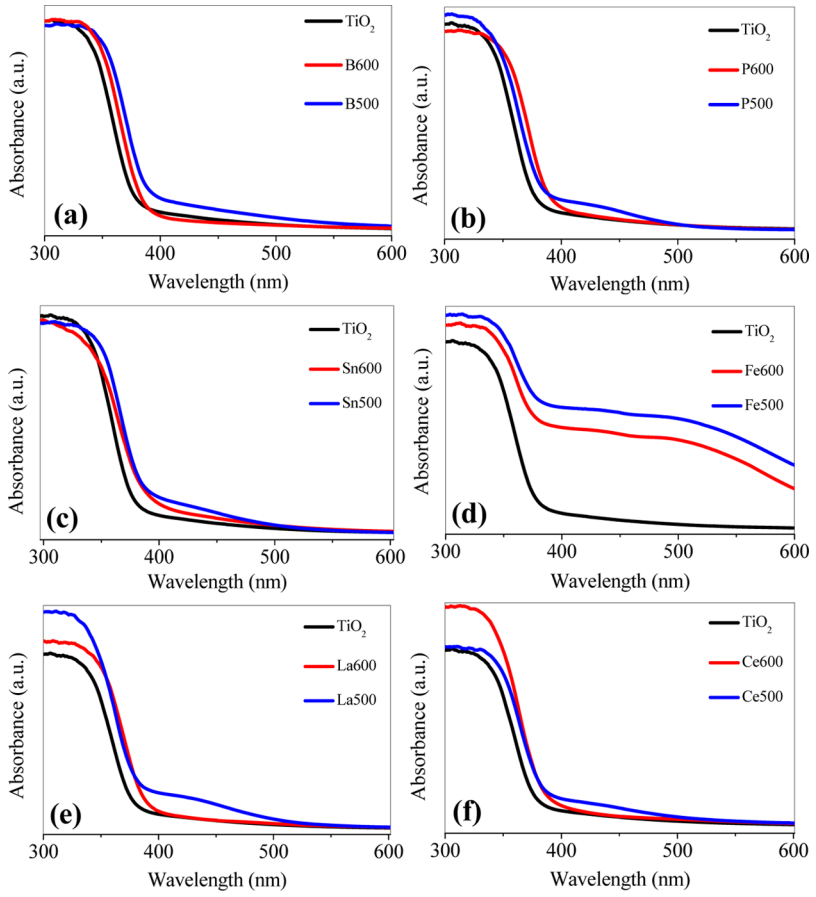

Figure 5. DRS spectra of the pure and doped TiO_2 SCs: (a) B-TiO_2, (b) P-TiO_2, (c) Sn-TiO_2, (d) Fe-TiO_2, (e) La-TiO_2, and (f) Ce-TiO_2.

found, which intrinsically indicates that Ce_2O_3 might be amorphous (Figure 3f).[42] Considering that no cerium oxide phase was observed in the XRD spectrum (Figure 2), the Ce−O bonds were dispersive in or on the TiO_2 SCs and did not assemble to the cerium oxide phase. The Ce incorporation influenced both the lattice structure and the crystalline size. Because the ionic radius of Ce^{3+}/Ce^{4+} (1.03/0.93 Å) is between Ti^{4+} (0.68 Å) and O^{2-} (1.32 Å), Ce could reside in the TiO_2 lattice interstitially or substitutionally.[42] The decreased crystalline size might be owning to the less reactive Ce ions, slowing down the condensation and crystallization of the titania matrix.

Moreover, when the doping temperature reduced from 600 to 500 °C, the as-prepared TiO_2 SCs were efficiently codoped by the added atom and the in situ N atom from the wasted anodic electrolyte (Figure S2, Supporting Information). With this synergistic codoping, the electrochemical, photochemical, and photocatalytic properties of the TiO_2 SCs could be further enhanced, compared to those of the samples prepared at 500 °C.

Electronic Properties of the Doped TiO_2 SCs. TiO_2 SCs electrodes were fabricated by drop-casting SCs onto fluorine doped tin oxide (FTO) substrates. The measured smaller arc radius on the modified TiO_2 SCs electrode clearly exhibited their enhanced electrochemical conductivity, reduced electron transfer resistance, and magnified the separation and transfer of electro-generated carriers because of their smaller arc radius, compared to the pure analogue (Figure 4a).[43] From the measured Mott−Schottky plots (Figure 4b), the positive slopes indicate the *n*-type behavior of both the pristine and modified TiO_2 SCs; on the other hand, the extracted flat-band potential (E(fb)) for the pristine TiO_2 SCs was approximately +0.2 V vs Ag/AgCl, which was obviously more negative than those of the doped analogues, and the larger slopes of the doped TiO_2 SCs suggest a significantly higher carrier density and a better electric conductivity compared to that of the undoped analogue. The low carrier density of the pure TiO_2 SCs reflects their high crystalline quality, resulting from the high temperature used in the thermal synthesis.[2]

TiO_2 can be used for water photoelectrolysis, while its large overpotential for the oxygen evolution reaction (OER) usually limits its efficient application. Because this OER overpotential is affected by the binding energy with intermediates such as O·, HO·, and HOO·, a stronger interaction among the adsorbed species on the surface can lead to a lower overpotential. Recently, it has been reported that the introduction of foreign dopants uniformly into the TiO_2 lattice can substantially decrease the apparent overpotential and significantly increase the overall catalytic performance.[2,44] As shown in Figure 4c and Table S1 (Supporting Information), the doped TiO_2 SCs exhibited a substantially reduced overpotential for OER than that on the pristine samples, implying that impurity doping on TiO_2 crystals was able to alter the adsorption energy of reaction intermediates for OER despite the low quantity of dopant. Moreover, such a change in the surface adsorption energy is intrinsically governed by the type of the foreign dopants and by its doping position in the crystal lattice.[2,44]

Although the quantitative determination of OER overpotential was highly current-dependent, the trend could be compared in the following order: Ce-TiO_2 < La−N−TiO_2 <

Ce−N−TiO_2 < Sn−N−TiO_2 < P−N−TiO_2 < Fe−N−TiO_2 < B−N−TiO_2 < La-TiO_2 < B-TiO_2 < P-TiO_2 < Sn-TiO_2 < Fe-TiO_2 < TiO_2. At the selected current of 0.45 μA, an overpotential of 0.66 V was obtained on 3% Ce-doped TiO_2 SCs, which exhibited a ∼60% decrease relative to that of the pure TiO_2 SCs (1.28 V) (Figure 4d).

Photocatalytic Degradation of RhB. The DRS is one of the most widely used methods to evaluate the optical properties of photocatalysts and examine the doping effects on the host metal oxide matrix. Figure 5 shows that all of the doped TiO_2 SCs prepared at 600 °C exhibited a stronger adsorption than the pristine analogue above ca. 380 nm (3.20 eV, corresponding to the intrinsic band gap adsorption of TiO_2).[45] On the one hand, it was noted that the absorption band shifted smoothly toward the visible light region, and the extent of this red shift in absorption band was highly dependent on the type and amount of foreign dopants (Figure 5). These facts indicate that the photonic bandgap of the as-prepared TiO_2 SCs was intrinsically changed after foreign doping at 600 °C.[45] On the other hand, for the La- and Ce-doped samples, although most of the La_2O_3 and Ce_2O_3 were present in a separated phase adsorbed onto the TiO_2 SCs, their presence could also promote light harvesting due to the enhanced surface area.[40] Meanwhile, La_2O_3 and Ce_2O_3 could capture photoelectrons and inhibit their recombination with holes, which might further enhance light absorbance in both UV and visible regions.[46] In addition, the drastic visible light adsorption on the Fe-doping TiO_2 SCs was consistent with the changes from white to yellow or light brown in the sample color (Figure 1). In principle, this strong adsorption could be mainly attributed to the two following mechanisms: the excitation of 3d electrons of Fe^{3+} to the TiO_2 conduction band (charge transfer transition), which gives rise to an absorption band centered at ca. 400 nm, and the $d-d$ transition of Fe^{3+} ($^2T_{2g} \rightarrow {}^2A_{2g}$, $^2T_{1g}$) or the charge transfer transition between the interacting iron ions ($Fe^{3+} + Fe^{3+} \rightarrow Fe^{4+} + Fe^{2+}$).[40]

Moreover, for all of the doped samples prepared at 500 °C, an additional strong visible light absorption was observed at 400−500 nm (Figure 5). Compared to the doped TiO_2 SCs prepared at 600 °C, it was noted that the adsorption band remained intrinsically unchanged without any obvious shift, and only an additional visible light absorption shoulder centered at ca. 450 nm was formed on the doped TiO_2 SCs prepared at 500 °C. These two facts synergistically indicate that the photonic bandgap of the doped TiO_2 SCs was not intrinsically changed when the doping temperature was reduced from 600 to 500 °C.[28,45] The newly formed adsorption shoulder peak on the doped TiO_2 SCs prepared at 500 °C might be mainly attributed to the introduction of some localized states near the valence band edge to form an impurity energy level within the bandgap as well as the possible increase in surface oxygen vacancies and/or crystal defects from the crystallographical distortion of anatase crystalline lattice induced by N efficient doping.[47,48] Therefore, these results clearly suggest that the electric properties of the as-prepared TiO_2 SCs were effectively modified in different ways, and thus the intrinsic mechanisms for the modification of optical absorption properties through doping were highly different at the two given doping temperatures of 500 and 600 °C.

The measured transient photocurrents on all the doped TiO_2 SCs were significantly higher than those on the pristine ones under visible light irradiation, and the highest photocurrent was obtained on the P and N codoped sample prepared at 500 °C (Figures 6a and S2, Supporting Information). These results reveal an improved optical absorption and a decreased electron−hole recombination of the doped crystals.

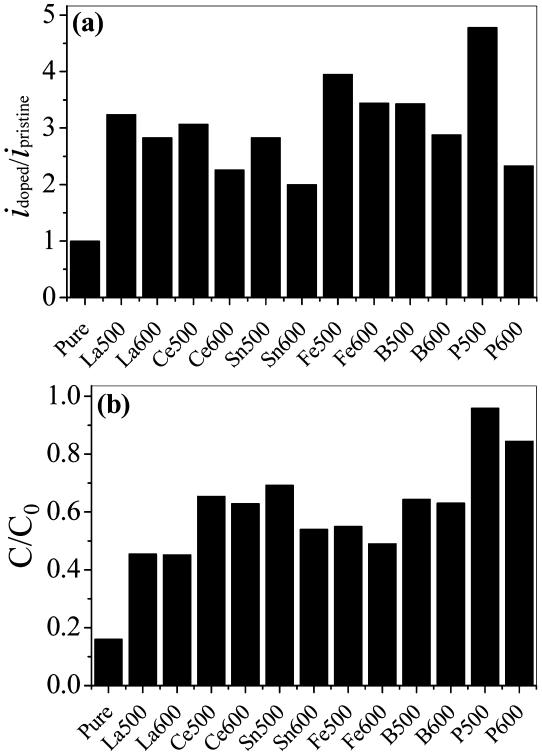

Figure 6. Photocatalytic degradation of (a) RhB and (b) transient photoresponse on the pure and modified TiO_2 SCs under visible light irradiation.

RhB, a widely used azo dye in printing and dyeing industries, was used as a model pollutant to evaluate the photoactivities of both the pristine and doped TiO_2 SCs under the visible light. The pristine SCs exhibited the lowest activity because of the large band gap, and the observed removal should be attributed to the self-sensitization of RhB (Figure 6b and Table S2, Supporting Information). In comparison, all the doped samples exhibited a significantly enhanced RhB removal efficiency (ca. 50−100%) owing to the desirable modifications of both crystal and electric structures (Figure 6b and Table S2, Supporting Information). Other mechanisms have been proposed to explain such an enhanced photoactivity. For example, the high activity of the B-doped sample can be due to the midgap band arising from the substitutional B for oxygen atoms, interstitial B, and the formation of localized oxygen vacancies.[49] The high activity of the Fe-doped sample can be ascribed to the narrowed band gap, the reduced electron−hole recombination, the increased flat-band potential, and donor density upon effective substitutional introduction of Fe^{3+} via the modifications in the electron−hole handling properties.[50] These results confirm an enhanced photoactivity on the doped crystals.

Moreover, the codoped TiO_2 SCs with N and other nonmetal elements usually exhibit favorable photocatalytic properties for the synergetic effect of the two dopants. In this study, the P, N codoped TiO_2 SCs exhibited a substantially higher RhB degradation (nearly 100%) than the P-doped sample (Figure 6b and Table S2, Supporting Information). According to the XPS analysis, the chemical natures of N and P

were identified as N−Ti−O and Ti−O−P, respectively, in the single-doped TiO_2 lattice, while the N (1.71%) was bonded to P to form the O−P−N linkage in the codoped analogue (Figure S2b, Supporting Information), which might result in the observed high activity.[38] This conclusion could be extended to some other foreign atoms, and is of considerable interests for the efficient photocatalytic water purification.

CONCLUSIONS

A facile and general approach is developed to dope and codope the {001}-exposed TiO_2 SCs by recycling wasted ethylene glycol anodic electrolyte from the TiO_2 nanotubes preparation process. Ce and La, Sn and Fe, and B and P are successfully doped into the facet-controlled TiO_2 SCs without changing their morphological and structural properties. Moreover, the synergistic codoping could be accomplished under appropriate conditions. The as-prepared doped TiO_2 SCs exhibit significantly enhanced electric properties, visible light utilization, and RhB degradation activity. Our findings provide a new opportunity for preparing the cost-effective modified TiO_2 SCs for efficient photocatalytic water treatment and other catalytic applications.

ASSOCIATED CONTENT

Supporting Information

FT-IR data, XPS spectrum for the codoping TiO_2 SCs, photocurrent curves, dopant concentration, and RhB degradation rate constants. This material is available free of charge via the Internet at http://pubs.acs.org.

AUTHOR INFORMATION

Corresponding Authors

*E-mail: aiyzhang@ustc.edu.cn. Fax: +86-551-63601592.
*E-mail: hqyu@ustc.edu.cn.

Notes

The authors declare no competing financial interest.

ACKNOWLEDGMENTS

The authors thank the National Basic Research Program of China (2011CB933702), the National Science Foundation of China (51208488), and the Program for Changjiang Scholars and Innovative Research Team in University of Ministry of Education of China for supporting this study.

REFERENCES

(1) Chen, X. B.; Mao, S. S. Titanium Dioxide Nanomaterials: Synthesis, Properties, Modifications, and Applications. *Chem. Rev.* **2007**, *107*, 2891−2959.
(2) Liu, B.; Chen, H. M.; Liu, C.; Andrews, S. C.; Hahn, C.; Yang, P. D. Large-Scale Synthesis of Transition-Metal-Doped TiO_2 Nanowires with Controllable Overpotential. *J. Am. Chem. Soc.* **2013**, *135*, 9995−9998.
(3) Asahi, R.; Morikawa, T.; Ohwaki, T.; Aoki, K.; Taga, Y. Visible-Light Photocatalysis in Nitrogen-Doped Titanium Oxides. *Science* **2001**, *293*, 269−271.
(4) Yu, J. C.; Ho, W.; Yu, J. G.; Yip, H.; Wong, P. K.; Zhao, J. C. Efficient Visible-Light-Induced Photocatalytic Disinfection on Sulfur-Doped Nanocrystalline Titania. *Environ. Sci. Technol.* **2005**, *39*, 1175−1179.
(5) Liu, H. M.; Imanishi, A.; Nakato, Y. Mechanisms for Photooxidation Reactions of Water and Organic Compounds on Carbon-Doped Titanium Dioxide, as Studied by Photocurrent Measurements. *J. Phys. Chem. C* **2007**, *111*, 8603−8610.
(6) Zhou, J. K.; Lv, L.; Yu, J. Q.; Li, H. L.; Guo, P. Z.; Sun, H.; Zhao, X. S. Synthesis of Self-Organized Polycrystalline F-Doped TiO_2 Hollow Microspheres and Their Photocatalytic Activity under Visible Light. *J. Phys. Chem. C* **2008**, *112*, 5316−5321.
(7) Lu, N.; Quan, X.; Li, J. Y.; Chen, S.; Yu, H. T.; Chen, G. H. Fabrication of Boron-Doped TiO_2 Nanotube Array Electrode and Investigation of Its Photoelectrochemical Capability. *J. Phys. Chem. C* **2007**, *111*, 11836−11842.
(8) Xing, M. Y.; Wu, Y. M.; Zhang, J. L.; Chen, F. Effect of Synergy on the Visible Light Activity of B, N, and Fe Co-Doped TiO_2 for the Degradation of MO. *Nanoscale* **2010**, *2*, 1233−1239.
(9) Wang, Y. D.; Chen, T.; Mu, Q. Y. Electrochemical Performance of W-Doped Anatase TiO_2 Nanoparticles as an Electrode Material for Lithium-Ion Batteries. *J. Mater. Chem.* **2011**, *21*, 6006−6013.
(10) Matsumoto, Y.; Murakami, M.; Shono, T. Room-Temperature Ferromagnetism in Transparent Transition Metal Doped Titanium Dioxide. *Science* **2001**, *291*, 854−856.
(11) Tsuyumoto, I.; Nawa, K. Thermochromism of Vanadium-Titanium Oxide Prepared from Peroxovanadate and Peroxotitanat. *J. Mater. Sci.* **2008**, *43*, 985−988.
(12) Li, J.; Zeng, H. C. Hollowing Sn-Doped TiO_2 Nanospheres via Ostwald Ripening. *J. Am. Chem. Soc.* **2007**, *129*, 15839−15847.
(13) Ramakrishma, G.; Das, A.; Ghosh, H. N. Effect of Surface Modification on Back Electron Transfer Dynamics of Dibromo Fluorescein Sensitized TiO_2 Nanoparticles. *Langmuir* **2004**, *20*, 1430−1435.
(14) Ma, T. Y.; Cao, J. L.; Shao, G. S.; Zhang, X. J.; Yuan, Z. Y. Hierarchically Structured Squama-Like Cerium-Doped Titania: Synthesis, Photoactivity, and Catalytic CO Oxidation. *J. Phys. Chem. C* **2009**, *113*, 16658−16667.
(15) Liu, H.; Yu, L. X.; Chen, W. F.; Li, Y. Y. The Progress of TiO_2 Nanocrystals Doped with Rare Earth Ions. *J. Nanomater.* **2012**, DOI: 10.1155/2012/235879.
(16) Dai, K.; Peng, T. Y.; Chen, H. Photocatalytic Degradation of Commercial Phoxim over La-Doped TiO_2 Nanoparticles in Aqueous Suspension. *Environ. Sci. Technol.* **2009**, *43*, 1540−1545.
(17) Chevallier, L.; Bauer, A.; Cavaliere, S.; Hui, R.; Roziere, J.; Jones, D. J. Mesoporous Nanostructured Nb-Doped Titanium Dioxide Microsphere Catalyst Supports for PEM Fuel Cell Electrodes. *ACS Appl. Mater. Interfaces* **2012**, *4*, 1752−1759.
(18) Liu, G.; Sun, C. H.; Wang, L. Z.; Smith, S. C.; Lu, G. Q.; Cheng, H. M. Bandgap Narrowing of Titanium Oxide Nanosheets: Homogeneous Doping of Molecular Iodine for Improved Photoreactivity. *J. Mater. Chem.* **2011**, *21*, 14672−14679.
(19) Jing, L. Q.; Xin, B. F.; Yuan, F. L.; Xue, L. P.; Wang, B. Q.; Fu, H. G. Effects of Surface Oxygen Vacancies on Photophysical and Photochemical Processes of Zn-Doped TiO_2 Nanoparticles and Their Relationships. *J. Phys. Chem. B* **2006**, *110*, 17860−17865.
(20) Yu, J. G.; Xiang, Q. J.; Zhou, M. H. Preparation Characterization and Visible-Light-Driven Photocatalytic Activity of Fe-Doped Titania Nanorods and First-Principles Study for Electronic Structures. *Appl. Catal., B* **2009**, *90*, 595−603.
(21) Narayan, H.; Alemu, H.; Macheli, L.; Thakurdesai, M. Synthesis and Characterization of Y^{3+}-Doped TiO_2 Nanocomposites for Photocatalytic Applications. *Nanotechnology* **2009**, *20*, 255601−255609.
(22) Nagaveni, K.; Hegde, M. S.; Madras, G. Structure and Photocatalytic Activity of $Ti_{1-x}M_xO_2^+$/-delta (M = W, V, Ce, Zr, Fe, and Cu) Synthesized by Solution Combustion Method. *J. Phys. Chem. B* **2004**, *108*, 20204−20212.
(23) Kesselman, J. M.; Weres, O.; Lewis, N. S.; Hoffmann, M. R. Electrochemical Production of Hydroxyl Radical at Polycrystalline Nb-Doped TiO_2 Electrodes and Estimation of the Partitioning between Hydroxyl Radical and Direct Hole Oxidation Pathways. *J. Phys. Chem. B* **1997**, *101*, 2637−2643.
(24) Liu, G.; Yang, H. G.; Pan, J.; Yang, Y. Q.; Lu, G. Q.; Cheng, H. M. Titanium Dioxide Crystals with Tailored Facets. *Chem. Rev.* **2014**, DOI: 10.1021/cr400621z.

(25) Liu, S. W.; Yu, J. G.; Jaroniec, M. Anatase TiO_2 with Dominant High-Energy {001} Facets: Synthesis, Properties, and Applications. *Chem. Mater.* **2011**, *23*, 4085−4093.
(26) Pan, J.; Liu, G.; Lu, G. Q.; Cheng, H. M. On the True Photoreactivity Order of {001}, {010}, and {101} Facets of Anatase TiO_2 Crystals. *Angew. Chem., Int. Ed.* **2011**, *50*, 2133−2137.
(27) Zhang, A. Y.; Long, L. L.; Li, W. W.; Wang, W. K.; Yu, H. Q. Hexagonal Microrods of Anatase Tetragonal TiO_2: Self-Directed Growth and Superior Photocatalytic Performance. *Chem. Commun.* **2013**, *49*, 6075−6077.
(28) Liu, G.; Yang, H. G.; Wang, X. W.; Cheng, L. N.; Pan, J.; Lu, G. Q.; Cheng, H. M. Visible Light Responsive Nitrogen Doped Anatase TiO_2 Sheets with Dominant {001} Facets Derived from TiN. *J. Am. Chem. Soc.* **2009**, *131*, 12868−12869.
(29) Xiang, Q. J.; Yu, J. G.; Wang, W. G.; Jaronie, M. Nitrogen Self-Doped Nanosized TiO_2 Sheets with Exposed {001} Facets for Enhanced Visible-Light Photocatalytic Activity. *Chem. Commun.* **2011**, *47*, 6906−6908.
(30) Xiang, Q. J.; Yu, J. G.; Jaroniec, M. Nitrogen and Sulfur Co-Doped TiO_2 Nanosheets with Exposed {001} Facets: Synthesis, Characterization, and Visible-Light Photocatalytic Activity. *Phys. Chem. Chem. Phys.* **2011**, *13*, 4853−4861.
(31) Zong, X.; Xing, Z.; Yu, H. Photocatalytic Water Oxidation on F, N Co-Doped TiO_2 with Dominant Exposed {001} Facets under Visible Light. *Chem. Commun.* **2011**, *47*, 11742−11744.
(32) Luo, W. Q.; Fu, C. Y.; Li, R. F. Er^{3+}-Doped Anatase TiO_2 Nanocrystals: Crystal-Field Levels, Excited-State Dynamics, Upconversion, and Defect Luminescence. *Small* **2011**, *7*, 3046−3056.
(33) Roy, P.; Berger, S.; Schmuki, P. TiO_2 Nanotubes: Synthesis and Applications. *Angew. Chem., Int. Ed.* **2011**, *50*, 2904−2939.
(34) Zhang, A. Y.; Long, L. L.; Yu, H. Q. Chemical Recycling of the Wasted Anodic Electrolyte from TiO_2 Nanotubes Preparation Process to Synthesize Facet-Controlled TiO_2 Single Crystals as an Efficient Photocatalyst. *Green Chem.* **2014**, *16*, 2745−2753.
(35) Iwasea, M.; Yamadaa, K.; Kurisakia, T.; Ohtanib, B.; Wakita, H. A study on the Active Sites for Visible-Light Photocatalytic Activity of Phosphorus-Doped Titanium(IV) Oxide Particles Prepared Using a Phosphide Compound. *Appl. Catal., B* **2013**, *140*, 327−332.
(36) Wei, J.; Zhu, W.; Zhang, Y. Q. An Efficient Two-Step Technique for Nitrogen-Doped Titanium Dioxide Synthesizing: Visible-Light-Induced Photodecomposition of Methylene Blue. *J. Phys. Chem. C* **2007**, *111*, 1010−1015.
(37) Chen, D.; Yang, D.; Wang, Q.; Jiang, Z. Effects of Boron Doping on Photocatalytic Activity and Microstructure of Titanium Dioxide Nanoparticles. *Ind. Eng. Chem. Res.* **2006**, *45*, 4110−4116.
(38) Lin, L. Synthesis and Characterization of Phosphor and Nitrogen Co-Doped Titania. *Appl. Catal., B* **2007**, *76*, 196−202.
(39) Aldon, L.; Kubiak, P.; Picard, A.; Jumas, J. C.; Fourcade, J. O. Size Particle Effects on Lithium Insertion into Sn-Doped TiO_2 Anatase. *Chem. Mater.* **2006**, *18*, 1401−1405.
(40) Adán, C.; Bahamonde, A.; Fernández-García, M.; Martínez-Arias, A. Structure and Activity of Nanosized Iron-Doped Anatase TiO_2 Catalysts for Phenol Photocatalytic Degradation. *Appl. Catal., B* **2007**, *72*, 11−17.
(41) Huo, Y. N.; Zhu, J.; Li, J. X.; Li, H. X. An Active La/TiO_2 Photocatalyst Prepared by Ultrasonication-Assisted Sol-Gel Method Followed by Treatment under Supercritical Conditions. *J. Mol. Catal. A: Chem.* **2007**, *278*, 237−243.
(42) Zhang, J.; Peng, W. Q.; Chen, Z. H.; Chen, H.; Han, L. Y. Effect of Cerium Doping in the TiO_2 Photoanode on the Electron Transport of Dye-Sensitized Solar Cells. *J. Phys. Chem. C* **2012**, *116*, 19182−19190.
(43) Hou, Y.; Zuo, F.; Dagg, A.; Feng, P. Y. A Three-Dimensional Branched Cobalt-Doped α-Fe_2O_3 Nanorod/$MgFe_2O_4$ Heterojunction Array as a Flexible Photoanode for Efficient Photoelectrochemical Water Oxidation. *Angew. Chem., Int. Ed.* **2013**, *53*, 1286−1290.
(44) Garcia-Mota, M.; Vojvodic, A.; Metiu, H.; Man, I. C.; Su, H. Y.; Rossemeisl, J.; Norskov, J. K. Tailoring the Activity for Oxygen Evolution Electrocatalysis on Rutile TiO_2 (110) by Transition-Metal Substitution. *ChemCatChem.* **2011**, *3*, 1607−1611.
(45) Liu, G.; Sun, C. H.; Smith, S. C.; Wang, L. Z.; Lu, G. Q.; Cheng, H. M. Sulfur Doped Anatase TiO_2 Single Crystals with a High Percentage of {001} Facets. *J. Colloid Interface Sci.* **2010**, *349*, 477−483.
(46) Huo, Y. N.; Zhang, X. Y.; Jin, Y.; Zhu, J.; Li, H. X. Highly Active La_2O_3/$Ti_{1-x}B_xO_2$ Visible Light Photocatalysts Prepared under Supercritical Conditions. *Appl. Catal., B* **2008**, *83*, 78−84.
(47) Guo, W.; Shen, Y. H.; Boschloo, G.; Hagfeldt, A.; Ma, T. Influence of Nitrogen Dopants on N-Doped TiO_2 Electrodes and Their Applications in Dye-Sensitized Solar Cells. *Electrochim. Acta* **2011**, *56*, 4611−4617.
(48) Guo, W.; Shen, Y. H.; Wu, L. Q.; Gao, Y. R.; Ma, T. L. Effect of N Dopant Amount on the Performance of Dye-Sensitized Solar Cells Based on N-Doped TiO_2 Electrodes. *J. Phys. Chem. C* **2011**, *115*, 21494−21499.
(49) Liu, J. W.; Han, R.; Wang, H. T.; Zhao, Y.; Lu, W. J.; Wu, H. Y.; Yu, T. F.; Zhang, Y. X. Degradation of PCP-Na with La-B Co-Doped TiO_2 Series Synthesized by the Sol-Gel Hydrothermal Method under Visible and Solar Light Irradiation. *J. Mol. Catal. A: Chem.* **2011**, *344*, 145−152.
(50) Singh, A. P.; Kumari, S.; Shrivastav, R.; Dass, S.; Satsangi, V. R. Iron Doped Nanostructured TiO_2 for Photoelectrochemical Generation of Hydrogen. *Int. J. Hydrogen Energy* **2008**, *33*, 5363−5368.